Calculation of Low-Frequency Unsteady Behavior of Liquid Rockets from Droplet Combustion Parameters

W. T. WEBBER*
McDonnell Douglas Astronautics Company—West, Huntington Beach, Calif.

The transient behavior of the combustion chamber may be obtained by simultaneous digital integration of the differential equations describing liquid propellant flow through the feed system and injector, atomization of the injected streams, and aerodynamic drag, heat-transfer and evaporation rates of the individual propellant droplets, together with the time-varying thermochemical state of the chamber gas and the nozzle efflux rate. High-amplitude chugging instability was produced experimentally in a small rocket engine using a family of four injectors. The calculated values for amplitude and frequency differed from the experimental values by no more than 5% and 7%, respectively. Calculated start transients have agreed with experimental starts for a number of engines, having quite different characteristics, and have been useful in diagnosing start problems and correctly evaluating corrective measures.

Nomenclature

A = cross section area of feed lines, acceleration
C = heat capacity, coefficient
D = diameter
E = gas volume upstream of injector orifices
F = stoichiometry—fuel fraction
G = burning rate parameter $\pi k/Cp$
ΔH = heat to warm and evaporate unit mass of propellant
K = droplet axial velocity/stream velocity, droplet group diameter/median diameter
k = thermal conductivity
L = length of feed line segments
M = mass of a droplet
$\dot{M}$ = mass burning rate of a droplet, mass flow rate
$\dot{m}$ = mass injection rate of fuel or oxidizer
$\mathcal{M}$ = molecular weight of combustion gas
N = number of droplets in a group, dimensionless modulus
P = pressure
q = volumetric flow rate
R = coefficient for steady-flow pressure drop
$\mathcal{R}$ = universal gas constant
S = axial chamber distance where atomization is complete
T = temperature
t = time
U = complete or partial chamber volume
V = velocity
X = axial location of a droplet group
W = burning rate parameter $= Cp/\Delta H = \alpha/\Delta T$
α = burning rate parameter $Cp\ \Delta T/\Delta H$
γ = ratio of specific heats
ρ = density
σ = surface tension
μ = viscosity

Subscripts

C = chamber
D = drag
e = exit conditions
g = combustion gas
i = a particular group of droplets in the chamber
j = jet conditions
L = a particular axial location of the chamber
n = a particular droplet size group produced by the injector
Nu = Nusselt number
P = at constant pressure
Re = Reynolds number
T = throat
t = tank, time interval
x = component in the axial direction
30 = volume-number-mean

Received September 16, 1970; revision received November 8, 1971. This work was supported by McDonnell Douglas Astronautics Company Independent Research and Development funds.

* Engineer/Scientist Specialist.

Introduction

PAST attempts to analyze problems of startup, shutdown, throttling, pulse-mode operation, and chugging instability of liquid fuel rockets have often used grossly simplified mathematical descriptions of the combustion process in order to obtain closed-form solutions or simplified differential equations suitable for analog computation. These simplified methods are inadequate to predict amplitude, frequency, or waveform of transient phenomena and are unable to relate engine behavior to the basic engine and propellant parameters. The combustion chamber analyses of Priem, Heidmann[1] and others,[2] which are based upon the evaporation rates and trajectories of large ensembles of propellant droplets, are able to relate the combustor behavior to the measurable physical characteristics of the combustor and propellants; but these analyses have been restricted to steady flow in the combustor. Transverse acoustic instability models[3] calculate unsteady phenomena in a thin transverse slice of a chamber, but not unsteady behavior of the propulsion system as a whole. The present paper describes a method of calculating low-frequency unsteady combustor behavior based upon the evaporation and combustion rates of the propellant droplets, together with the other system processes.

The model consists of fuel and oxidizer supply systems, an injector, a combustion chamber, and a nozzle. The calculations are done by an Euler integration in which successive new values are obtained from the preceding value, the calculated rate of change and the integrating time interval. The sequence of events in the calculation is shown in Fig. 1.

Supply system calculations give the time-varying injection rate of each propellant component as a function of the changing chamber pressure, valve areas and initial void volumes in the flow passages. The injector calculations give the time-varying initial droplet sizes, initial velocities, and initial positions for the propellants entering the chamber. Combustion chamber calculations give the trajectories and evaporation rate histories for all of the droplets and follow each droplet group until it is consumed or escapes through the nozzle. The axial gas velocity profile in the chamber is calculated at each time interval in order to calculate the local velocity differences between droplets and gas. The thermodynamic state of the gas in the chamber is recalculated at each time interval and is used

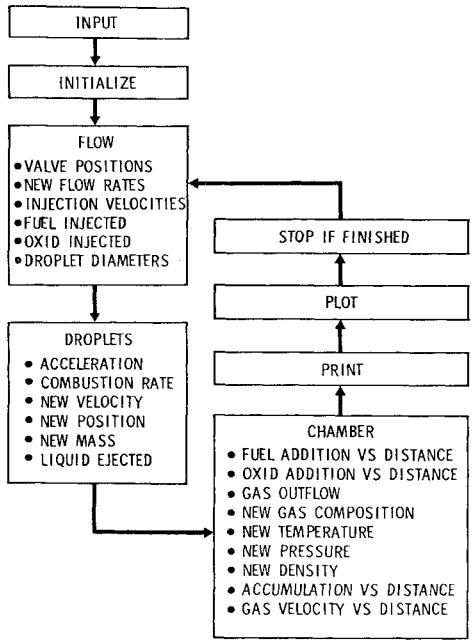

Fig. 1 Block diagram of calculations.

in the droplet, nozzle, and feed system calculations. Nozzle calculations give the rate of efflux of gas from the chamber in terms of time-varying pressure, temperature, mean molecular weight and thermal properties of the combustion chamber gas.

Feed System Calculations

The liquid propellant flow equations use a lumped parameter approximation incorporating only resistance and inertia terms

$$dq/dt = (P_t - P_c - (\tfrac{1}{2})R\rho q|q|)/(\rho \Sigma L/A) \tag{1}$$

L and A are the length and cross-sectional area for each segment in a sequence of series ducts having different cross-sectional areas. R is a coefficient chosen to approximate the summation of turbulent line losses and nozzle losses in the flow system, and is made time-dependent to model the opening and closing of propellant valves.

This flow equation implies that the compression of propellant in the flow passages is small and is adequate for propellant flow changes taking longer than five or six times the acoustic travel time of the duct. A more sophisticated method-of-characteristics approximation would be required to model very rapid pressure changes or very long propellant lines. When the injector is initially incompletely filled with liquid, or if gas is introduced by reverse flow during the course of a run, the void volume is calculated

$$E_{(t+\Delta_t)} = E_{(t)} - q\Delta t \tag{2}$$

where E is limited to values not less than zero. When the void volume has a positive value (i.e., when there is gas behind the injector) the values for R and $\Sigma L/A$ are modified to delete the resistance or inertia of the elements which are no longer liquid-filled.

Injector Calculations

If the instantaneous supply system flow rates of the fuel and oxidizer are positive and if the injector void volume is zero, the mass injection rate of either propellant is

$$\dot{m} = \rho q \tag{3}$$

If the void volume has a positive value, or if the supply system flow rate is negative, the corresponding mass injection rate is set equal to zero. The velocities of the injected streams are calculated

$$V_j = \dot{m}/\rho A \tag{4}$$

where V_j is the velocity along the axis of the jet, and A is the effective total cross-sectional area of the appropriate injector orifices. The initial axial velocity of the droplets produced from the stream is

$$V_x = KV_j \tag{5}$$

The coefficient K includes the effects of nonaxial injection as well as any injection nozzle velocity coefficients or velocity losses occurring in the atomization process.

The primary atomization process is approximated by calculating a time-varying median initial droplet size as a function of orifice diameter, instantaneous injection velocity, and propellant physical properties. The continuous distribution about this median droplet size in the real combustor is approximated in the model by creating five discrete groups of droplets having appropriate variations in size.

Experimental correlations are used to specify the median droplet size as a function of injection conditions. The correlation of Ingebo[4] for a self-impinging doublet using heptane shows

$$D_{30} = D_j/[0.3(D_jV_j)^{1/2} + 0.0125\ D_j\Delta V] \tag{6}$$

where D_{30} is the volume-number-mean droplet diameter, D_j is the injector orifice diameter, V_j is the injection velocity and ΔV is the velocity difference between the injected streams and the gas flow at the atomization point. It has been reported[1] that for rocket-engine conditions, where ΔV varies with axial distance from the injector, that 4560 cm/sec (150 fps) is an appropriate average value to use for ΔV.

The mean droplet diameter varies with the surface tension σ, viscosity μ, and density ρ of the injected fluid, an approximate relationship being[1]

$$D_A/D_B = (\rho_B\sigma_A\mu_A/\rho_A\sigma_B\mu_B)^{1/4} \tag{7}$$

for fluids A and B. Equations (6 and 7) are combined, along with the above value for ΔV, the physical properties of heptane and the multiplier need to convert from D_{30} to mass median diameter $\bar{D}$. This yields a more general expression for initial median droplet diameter expected from a self-impinging doublet injecting a fluid of specified properties

$$\bar{D} = 8.63(\sigma\mu/\rho)^{1/4}D_j/[(D_jV_j)^{1/2} + 195\ D_j] \tag{8}$$

The droplet size distribution about the median value is approximated by dividing the injected mass of each propellant into five equal portions. Each of these portions is converted to a group of droplets having a diameter which is a prescribed multiple of the median droplet diameter. The droplet group size ratios come from a table of coefficients chosen to approximate the experimental droplet size distribution. The droplet diameter, mass per droplet, and number of droplets for the nth group are

$$D_n = \bar{D}K_n,\ M_n = \rho(\pi/6)D_n^3,\ N_n = 0.2\dot{m}\Delta t/M_n \tag{9}$$

The coefficients used to represent two different drop-size distributions are given in Table 1.

Table 1 Droplet diameter distributions, midquintile diameter/median diameter

	Ingebo experimental	Log-probability $\sigma = 2.4$
K_1	0.198	0.333
K_2	0.759	0.645
K_3	1.00	1.00
K_4	1.23	1.55
K_5	2.30	3.00

Combustion Chamber Calculations

The eleven parameters used to represent the properties of each droplet group i are M_i, N_i, ρ_i, V_i (axial velocity), X_i (axial location), F_i (mass fraction of the droplet which is fuel), T_i (typical surface temperature), G_i (first burning rate parameter), W_i (second burning rate parameter), S_i (axial location where atomization is complete), $\dot{M}_i$ (computed burning rate of this droplet this time interval) $i = 1, 2, \ldots, n$ and $n \leq 1000$. The transient behavior of the rocket can be adequately modelled using no more than 1000 droplet groups at any one time, so the computer storage requirement for these droplet properties is 11,000 locations. The storage locations are reused for a newly injected droplet group when they are no longer required for the previous group, i.e., when the mass per droplet falls to zero or when the axial location increases to the total length of the combustion chamber. When a newly-injected droplet group enters the combustion chamber, its initial axial location is set to a value corresponding to the injection point of the injector, and the mass per droplet etc., are the values obtained from the flow system and atomization calculations previously described. It is presumed that the injector introduces all of the fuel and all of the oxidizer at single axial locations, and that it has only a single fuel orifice size, a single oxidizer orifice size, and single resultant stream angles. Thus only ten new droplet groups are introduced into the chamber each integrating time interval (five fuel size-groups and five oxidizer size-groups).

Impingement Distance and Breakup Distance

When the injected fluid first enters the chamber it is in the form of a coherent stream. Droplets are not formed until after the streams impinge and distort into sheets, ligaments and finally droplets. The exposed surface area of the fluid is relatively small until this primary atomization process is complete. To model this preatomization condition of the propellants, a value is calculated which is the axial distance from the injector corresponding to the geometrical impingement distance plus the distance required for the breakup to be completed following impingement. When the axial location of the injected droplet group is less than this value, the acceleration and burning rate of the droplets in the group is set equal to zero.

The effect of this breakup distance has proven to be of great importance to the calculations. The first propellant to enter the chamber after the valve starts to open is moving very slowly, because of the restriction of the valve and the inertia of the fluid in the line. The material which enters the chamber a few milliseconds later is moving much faster and tends to catch up with the material which was injected earlier. This "bunching" of the propellant causes the calculated impingement rate or droplet production rate to have a variation with time which is distinctively different from the injection rate. This may be seen from Fig. 4, which shows fuel line flow rate and the fuel impingement rate during chugging instability. There is inadequate experimental characterization of the breakup distance as a function of injection parameters. The present program takes a non-time-varying value from the correlation of Heidmann, Priem and Humphrey[5] based on the mean injection velocity. Attempts to use this correlation on a time-varying basis give results which disagree with experiment.

Droplet Motion Calculations

In general, the droplets in a droplet group at an axial location X_i will not be moving at the same velocity as the combusion product gas at that axial location. Near the injector face the droplets move faster than the gas while further down the chamber the gas moves faster than the droplets. The resultant aerodynamic drag force on each droplet will accelerate it. In order to calculate the aerodynamic accelerations, the droplet Reynolds number is calculated from

$$N_{Re} = \rho_g D_i | V_g - V_i | / \mu_g \tag{10}$$

where

$$D_i = (6 M_i / \pi \rho_i)^{1/3} \tag{11}$$

If $N_{Re} < 0.5$, the Stokes law acceleration is calculated

$$A = 18 \mu_g (V_g - V_i) / \rho_i D_i^2 \tag{12}$$

If $N_{Re} > 0.5$, the acceleration is calculated from the Newtonian drag law

$$A = 0.75 C_D \rho_g (V_g - V_i) | V_g - V_i | / \rho_i D_i \tag{13}$$

The drag coefficient correlation of Rabin[6] is approximated by the functions

$$0.5 < N_{Re} < 70 \quad C_D = 27 N_{Re}^{-0.84} \tag{14}$$

$$70 < N_{Re} < 59{,}000 \quad C_D = 0.414 N_{Re}^{0.1433} \tag{15}$$

$$59{,}000 < N_{Re} C_D = 2.0 \tag{16}$$

The new velocity and location of the droplet group are calculated from

$$V_{i(t+\Delta t)} = V_{i(t)} + A \Delta t \tag{17}$$

$$X_{i(t+\Delta t)} = X_{i(t)} + V_{i(t)} \Delta t + A (\Delta t)^2 / 2 \tag{18}$$

Droplet Evaporation Rate Calculations

The evaporation rate of a stable fuel or oxidizer droplet is largely determined by the processes of heat transport to the droplet surface and molecular diffusion away from it. For a large droplet, which has internal circulation, the transport of heat from its surface to its interior is also important. However, for the present calculations, the simplifying assumption is made that there is no heat transfer into the interior of any of the droplets. This permits accurate calculations for the small, noncirculating droplets which are responsible for much of rocket transient behavior, at the expense of accuracy in modelling the large droplets which largely determine combustion efficiency.

From the assumption that all heat reaching the surface of the droplet goes to evaporate liquid, the rate of evaporation is

$$\dot{M} = q / \Delta H = N_{Nu} \pi k D \Delta T / \Delta H \tag{19}$$

where q is the heat-transfer rate, N_{Nu} is the Nusselt number for heat transfer and ΔH is the sum of the latent heat of the liquid and the sensible heat required to raise it from the injection temperature. For a noneffusing sphere in a nonconvective environment, $N_{Nu} = 2.0$, but the value for a droplet evaporating into a high-temperature environment is much lower. Godsave[7] gives a simple but adequate estimate for the heat transfer to a burning droplet, assuming that thermal conductivity and specific heat of the vapor film is constant. His equation may be rearranged

$$N_{Nu} = 2[\ln(1 + \alpha)] / \alpha \tag{20}$$

where

$$\alpha \equiv C_p \Delta T / \Delta H \tag{21}$$

The rate of fuel consumption from burning fuel-wetted spheres has been determined experimentally under forced convective conditions by several investigators.[8-10] These experimental values are correlated (Fig. 2) by the equation

$$(\dot{M} - \dot{M}_0) / \dot{M}_0 = 0.25 N_{Re}^{0.5} \tag{22}$$

where $\dot{M}_0$ and $\dot{M}$ are nonconvective and convective consumption rates. This is rearranged and combined with Eq. (19) and (20) to give

$$N_{Nu} = (2 + 0.5 N_{Re}^{0.5}) [\ln(1 + \alpha)] / \alpha \tag{23}$$

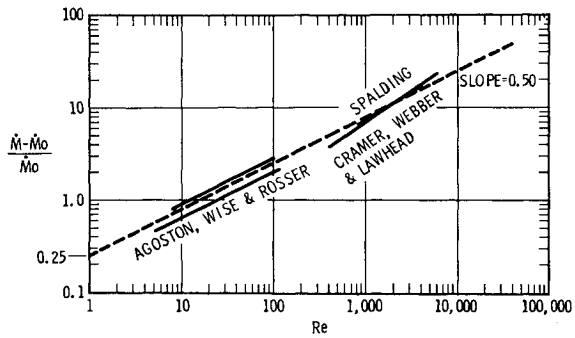

Fig. 2 Burning rate vs Reynolds number.

The term $(2 + 0.5\ N_{Re}{}^{0.5})$ represents the effect of forced convection on a burning sphere. It is similar in value to the correlation of Ranz and Marshall[11] for the rate of evaporation from wetted spheres, but is preferred for this application because it was obtained in the presence of combustion and with temperature differences up to 3000°K and Reynolds numbers up to 6000. The Ranz and Marshall experiments were limited to $\Delta T \leq 100$°K and $N_{Re} \leq 200$.

Equations (19) and (23) may be combined to give the burning rate of a droplet

$$\dot{M} = (\pi k/c_p)D(2 + 0.5\ N_{Re}{}^{0.5})\ln(1 + \alpha) \tag{24}$$

or

$$\dot{M}_i = G_i D_i(2 + 0.5\ N_{Re}{}^{0.5})\ln(1 + W_i \Delta T) \tag{25}$$

As previously noted, $G_i = (\pi k/c_p)$ and $W_i = c_p/\Delta H = \alpha/\Delta T$ are two of the subscripted variables characterizing each droplet group; these values are not treated as time-varying in the analysis in order to simplify the calculations. To obtain agreement with experimental burning rate values, c_p and k are evaluated at the arithmetic mean of the expected droplet surface and hot gas temperatures, $(T_i + T_g)/2$.

The ΔT used in the burning-rate equation is the difference between T_i and the flame temperature or gas temperature surrounding the droplet, T_g. For a volatile material, T_i is treated as nonvarying. For a high-boiling material it would be necessary to approximate T_i as a time-varying function of chamber pressure.

The value used for T_g is obtained from the curve of chamber temperature vs composition given in Fig. 3a, the calculated composition of the chamber gas F_g and the known composition of the droplet F_i. It is presumed that when a droplet of a given stoichiometry is evaporating into chamber gas having a different stoichiometry, every intermediate stoichiometry will be found in the diffusion zone surrounding the droplet and that the local temperature in the diffusion zone will correspond to the local stoichiometry. Thus, the T_g used in the burning-rate equation is the highest temperature found on $T(F)$ curve in the interval between $F = F_g$ and $F = F_i$.

Each time that the burning rate of a droplet is calculated from Eq. (25), the value is stored temporarily as a subscripted variable until it can be used in the summations which give the velocity profile in the chamber and the total burning rate for the chamber.

Use of Experimental Burning Rate Data

There are many common propellant materials for which the vapor thermal conductivity is unknown in the 1500°–2000°K temperature range. Nitric acid and UDMH are good examples. Since experimental droplet burning rates have been obtained for these materials, these burning rates may be used to infer this necessary information. Normally experimental burning rate data are given in terms of a burning rate constant K'

$$dD^2/dt = -K' \tag{26}$$

In terms of our droplet burning rate expression

$$K' = 8\ k\Delta T[\ln(1 + \alpha)]/\alpha\rho\Delta H \tag{27}$$

This expression is solved for k using the experimental value for K'. When the mean value for k is obtained this way, the droplet combustion equations are no longer being used to derive the burning rates from basic principles, but merely become functions for extending a burning rate measurement to different flame temperatures.

Gas State and Nozzle Flow

For simplicity the gas in the chamber is treated as an ideal gas and is assumed to be well mixed and in thermochemical equilibrium. The combustion is assumed to be isenthalpic. At any instant the gas in all parts of the chamber is presumed to be at the same pressure and to have uniform composition and density. The gas entering the nozzle is assumed to have the same composition, T, $\mathcal{M}$, and γ as the chamber gas. The flow of gas and droplets is assumed to be one-dimensional. It is assumed that the axial gas velocity profile can be approximated adequately by calculating the velocity at 100 equally spaced axial locations, with linear interpolation being used between the calculated values.

At each integration time interval, the droplet evaporation calculations and the nozzle flow equations are used to calculate the amount of fuel-derived mass and oxidizer-derived mass which have been added to the chamber gas through evaporation, and the amounts exhausted through the nozzle. The new amounts of fuel-derived gas mass and oxidizer-derived gas mass contained in the chamber are

$$M_{F(t+\Delta t)} = M_{F(t)} + \sum \dot{M}_i N_i F_i \Delta t - \dot{M}_F \Delta t \tag{28}$$

$$M_{o(t+\Delta t)} = M_{o(t)} + \sum \dot{M}_i N_i (1 - F_i)\Delta t - \dot{M}_o \Delta t \tag{29}$$

The total mass of gas in the chamber is

$$M_T = M_F + M_o \tag{30}$$

The fuel fraction of the chamber gas is

$$F_g = M_F/(M_F + M_o) \tag{31}$$

Since combustion product composition is only a weak function of pressure, the temperature, molecular weight, and thermal properties of the chamber gas are approximated as functions of F alone with only small error. Temperature, molecular weight and gamma are stored as 11-point tables with linear interpolation being used to obtain values for intermediate values of F. Figures 3a, 3b, and 3c illustrate the values used for the white fuming nitric acid–UDMH propellant combination.

Having $T_g(F)$ and $\mathcal{M}(F)$, the chamber pressure is calculated,

$$P_c = \rho \mathcal{R} T/\mathcal{M} = M_T \mathcal{R} T/\mathcal{M} U_c \tag{32}$$

where U_c is chamber volume.

Conventional steady flow, compressible gas, nozzle flow equations are used to calculate the instantaneous mass flow rate through the nozzle. The use of these equations together with the assumption of constant pressure throughout the chamber restricts the validity of these calculations to cases where the rate of change of pressure is sufficiently slow that only a small change in pressure occurs during a single acoustic time period of the chamber or nozzle.

The nozzle is sonic when

$$P_e/P_c \leq [2/(\gamma + 1)]^{\gamma/(\gamma-1)} \tag{33}$$

Subsonic mass flow rate is calculated

$$\dot{M}_T = A_T P_c[2\gamma\mathcal{M}/(\gamma - 1)\mathcal{R}T_c]^{1/2} \times [(P_e/P_c)^{2/\gamma} - (P_e/P_c)^{(\gamma+1)/\gamma}]^{1/2} \tag{34}$$

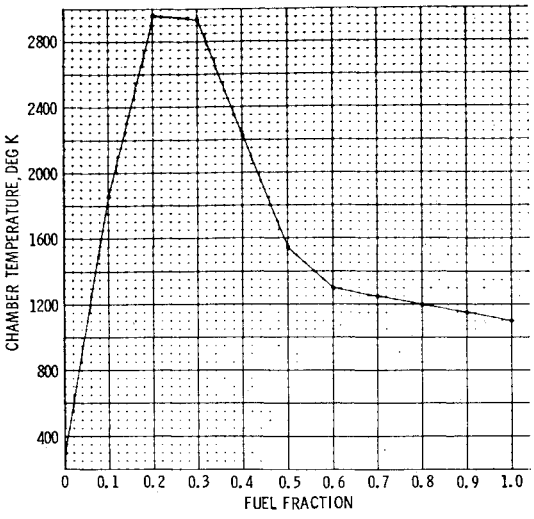

Fig. 3a Temperature vs stoichiometry.

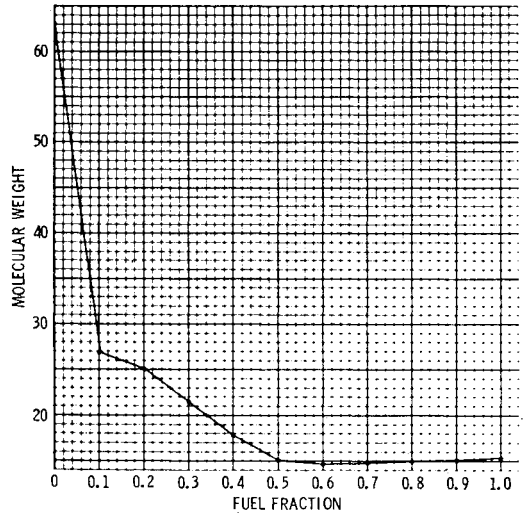

Fig. 3b Molecular weight vs stoichiometry.

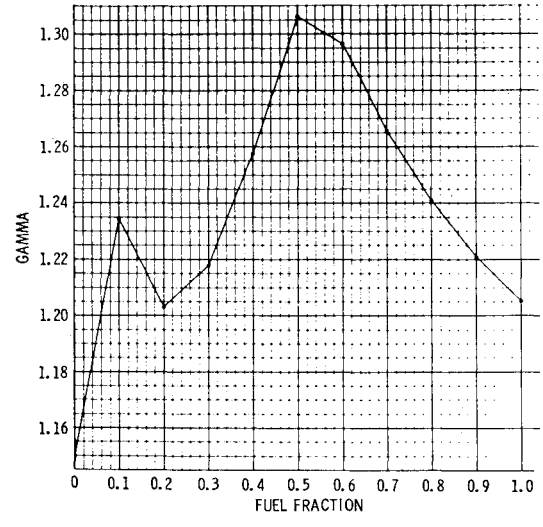

Fig. 3c Gamma vs stoichiometry.

Sonic flow rate is calculated

$$\dot{M}_T = A_T P_c \left[\frac{\gamma \mathcal{M}}{\mathcal{R} T_c}\left(\frac{2}{\gamma+1}\right)^{\frac{\gamma+1}{\gamma-1}}\right]^{1/2} \tag{35}$$

The rates at which fuel- and oxidizer-derived mass leave the chamber are

$$\dot{M}_F = \dot{M}_T \times F_g \tag{36}$$

$$\dot{M}_o = \dot{M}_T \times (1 - F_g) \tag{37}$$

Axial Gas Velocity

The axial gas velocity at any axial location L is

$$V_L = \dot{M}_L / \rho_g A_L \tag{38}$$

where

$\dot{M}_L$ = (Evaporation rate upstream of L) − (accumulation rate upstream of L) (39)

$$\dot{M}_L = \sum_{Xi \le L} \dot{M}_i N_i - U_L / U_c \left[\sum_{\text{all drops}} \dot{M}_i N_i - \dot{M}_T\right] \tag{40}$$

Where U_L is the chamber volume upstream of L. The simple form for the accumulation term depends upon the assumption of uniform density in the chamber gas.

Results Obtained

The numerical calculations are stable and appear to be negligibly influenced by the integrating time interval at the values which are used. Figure 4 illustrates the chamber pressure, fuel flow rate and impingement rates calculated for a 100-msec sequence of high-amplitude, 66 Hz, chugging instability. A 0.25 msec integrating time interval was used, which gives 60 calculated pressure points per cycle of instability. When these calculations were redone using a doubled time interval, the calculated amplitude changed by 0.2%, and the frequency changed by less than 3%. The computer time required for the calculations of Fig. 4 is between 2 and 3 min on a CDC 6500 computer.

The calculations appear to be insensitive to small changes in the droplet size distribution. The two distributions illustrated in Table 1 yield calculated chug parameters which differ by fractions of 1%. Gross changes in the drop-size distribution, such as omitting all the small or all the large droplets, cause drastic changes.

The form of the $T(F)$ curve (Fig. 3a) is important to the calculations. When the present 10-segment approximation is replaced by a 3-segment approximation, there are definite differences in the calculated frequencies and amplitudes.

The program calculations were tested by comparison with low-frequency combustion instability produced in a small experimental engine. The engine was operated with 4 injectors which differed only in impingement distance. The results are shown in Fig. 5. The calculated and experimental frequencies differed by no more than 7% while the amplitudes agreed within 5%. The calculated waveforms were similar to those obtained experimentally. In both cases the rate of rise of chamber pressure was considerably faster than the rate of fall and the curves were sharp-pointed at the minimum values. The periodic reversals of flow in the fuel line with backflow of gas through the injector ports each cycle were experimentally observed through a window in the injector body.

The start characteristics of the motor were calculated for various fuel and oxidizer "leads." The results of these calculations are shown in Fig. 6. Experimental verification is more qualitative in this case. Starts were found to be mild with no lead or acid lead, but destructive with a fuel lead.

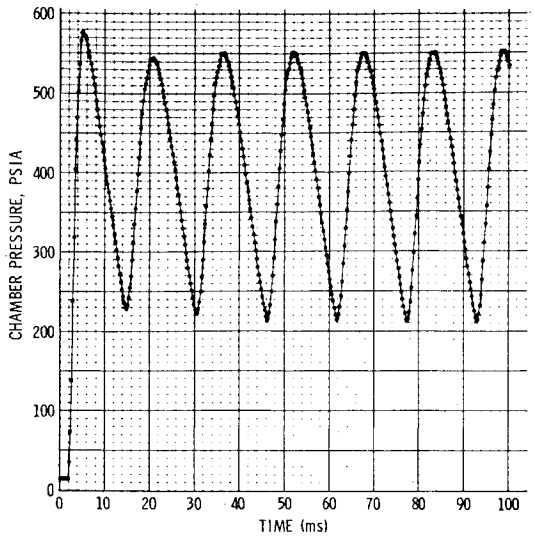

Fig. 4a Chamber pressure vs time.

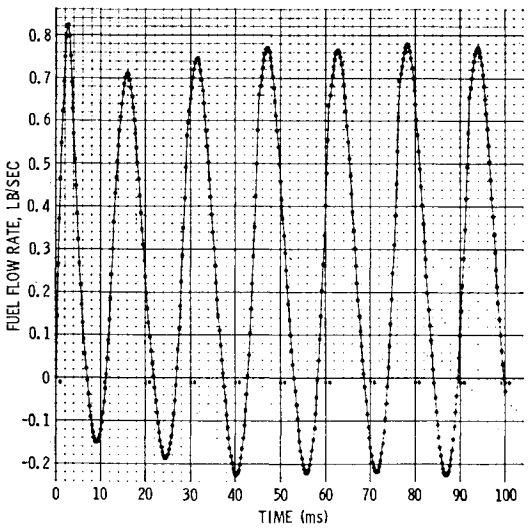

Fig. 4b Fuel flow rate vs time.

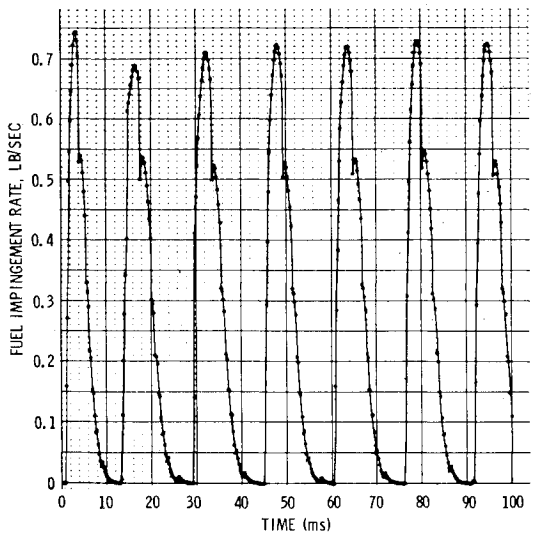

Fig. 4c Fuel impingement rate vs time.

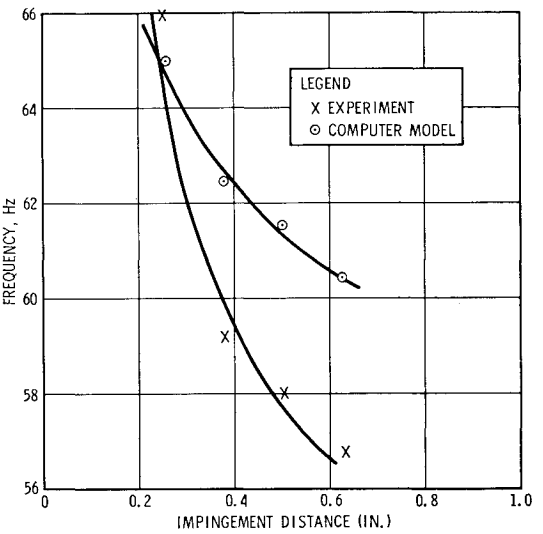

Fig. 5a Frequency vs impingement distance.

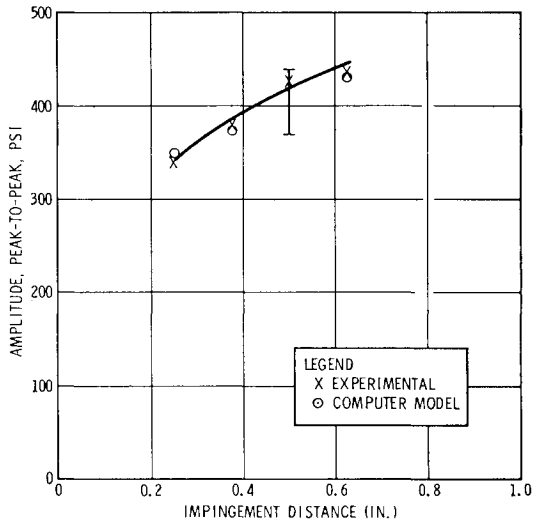

Fig. 5b Amplitude vs impingement distance.

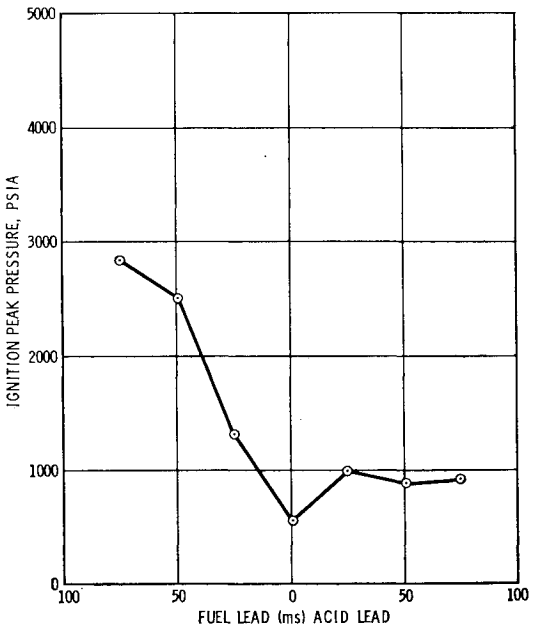

Fig. 6 Start pressure vs lead.

Practical Applications

The computer program has been of considerable assistance in correcting problems of new rocket-engine hardware. It has been used to diagnose correctly and eliminate start problems in both ignited and hypergolic start sequences using both cryogenic and storable propellants.

Although there have been no experiments available for comparison, no trouble has been encountered in calculating cycles of pulse-mode operation (Fig. 7).

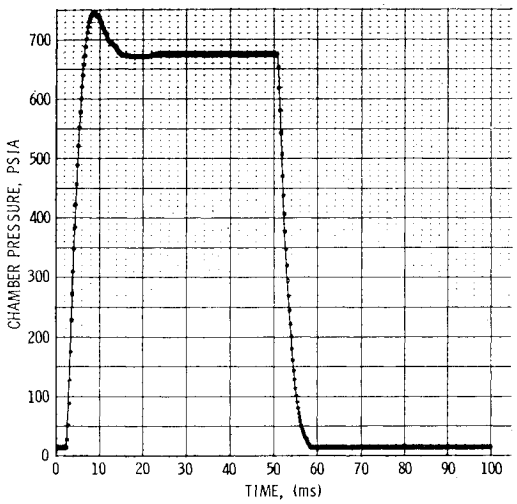

Fig. 7 Pulse-mode chamber pressure vs time.

References

[1] Priem, R. J. and Heidmann, M. F., "Propellant Vaporization as a Design Consideration for Rocket Engine Combustion Chambers," TR R-67, 1960, NASA.

[2] Lambiris, S., Combs, L. P., and Levine, R. S., "Stable Combustion Processes in Liquid Propellant Rocket Engines," *Combustion and Propulsion; Fifth AGARD Colloquium: High Temperature Phenomena*, Macmillan, New York, 1962.

[3] Hoffman, R. J., Wright, R. O., and Breen, B. P., "Combustion Instability Prediction Using a Non-linear Bipropellant Vaporization Model," Final Rept. NAS 7-442, Dynamic Science Corp. Monrovia, Calif., 1967.

[4] Ingebo, R. D., "Drop-Size Distributions for Impinging-Jet Breakup in Airstreams Simulating the Velocity Conditions in Rocket Combustors," TN 4222, 1958, NACA.

[5] Heidmann, M. E., Priem, R. J., and Humphrey, J. C., "A Study of Sprays Formed by Two Impinging Jets," TN 3835, 1957, NACA.

[6] Rabin, E., Schallenmueller, A. R., and Lawhead, R. B., "Displacement and Shattering of Propellant Droplets," AFOSR TR 60-75, 1960, Rocketdyne, Canoga Park, Calif.

[7] Godsave, G. A. E., "Studies of the Combustion of Drops in a Fuel Spray—The Burning of Single Drops of Fuel," *Fourth Symposium on Combustion*, Williams and Wilkins, Baltimore, Md., 1953.

[8] Spalding, D. B., "The Combustion of Liquid Fuels," *Fourth Symposium on Combustion*, Williams and Wilkins, Baltimore, Md., 1953.

[9] Agoston, G. A., Wise, H., and Rosser, W. A., "Dynamic Factors Affecting the Combustion of Liquid Spheres," *Sixth Symposium on Combustion*, Reinhold, New York, 1956.

[10] Webber, W. T., "Effects of Gas Motion on Heterogeneous Combustion, etc.," WADC TR 59-50, 1959, Rocketdyne, Canoga Park, Calif.

[11] Ranz, W. E. and Marshall, W. R., "Evaporation from Drops," *Chemical Engineering Progress*, Vol. 48, No. 4, 1952.

APRIL 1972 J. SPACECRAFT VOL. 9, NO. 4

Stability of Motion of Force-Free Spinning Satellites with Flexible Appendages

LEONARD MEIROVITCH*
Virginia Polytechnic Institute and State University, Blacksburg, Va.
AND
ROBERT A. CALICO†
University of Cincinnati, Cincinnati, Ohio

This paper presents two approaches to the stability analysis of torque-free spinning bodies consisting of a main rigid body and a number of distributed elastic parts. The stability analysis is based on the Liapunov direct method and takes into consideration automatically the existence of motion integrals. The first approach to the stability problem is based on modal analysis, whereas the second one makes use of integral coordinates. The case of a torque-free satellite represented by a rigid hub with six flexible appendages is solved. Closed-form stability criteria derived by the second approach compare favorably with numerical results obtained by modal analysis.

Introduction

THE rotational motion of a torque-free rigid body is known to be stable if the rotation takes place about an axis corresponding to either the maximum or the minimum moment of inertia, but the motion is unstable if the rotation takes place about the axis of intermediate principal moment of inertia [for example, Meirovitch (Ref. 1, Sec. 6.7)]. In general, however, spacecraft are not entirely rigid and the question remains as to what extent the rigid-body idealization can be justified.

Received September 7, 1971; revision received December 1, 1971. Presented as AAS Paper 71-345 at the AAS/AIAA Astrodynamics Specialists Conference, Ft. Lauderdale, Fla., August 17-19, 1971. This investigation has been supported by the NASA Research Grant NGR 36-004-042 sponsored by the Mechanical Systems Branch, Goddard Space Flight Center, whose support is gratefully acknowledged.

Index categories: Spacecraft Attitude Dynamics and Control; Structural Dynamic Analysis.

* Professor, Department of Engineering Mechanics. Formerly Professor, Department of Aerospace Engineering, University of Cincinnati. Member AIAA.

† Instructor, Department of Aerospace Engineering. Member AIAA.